JOURNAL OF GEOPHYSICAL RESEARCH: ATMOSPHERES, VOL. 119, 153–166, doi:10.1002/2013JD020537, 2014

Application of spectral analysis techniques in the intercomparison of aerosol data. Part II: Using maximum covariance analysis to effectively compare spatiotemporal variability of satellite and AERONET measured aerosol optical depth

Jing Li,[1,2] Barbara E. Carlson,[1] and Andrew A. Lacis[1]

Received 9 July 2013; revised 6 December 2013; accepted 10 December 2013; published 9 January 2014.

[1] Moderate Resolution Imaging SpectroRadiometer (MODIS) and Multi-angle Imaging Spectroradiomater (MISR) provide regular aerosol observations with global coverage. It is essential to examine the coherency between space- and ground-measured aerosol parameters in representing aerosol spatial and temporal variability, especially in the climate forcing and model validation context. In this paper, we introduce Maximum Covariance Analysis (MCA), also known as Singular Value Decomposition analysis as an effective way to compare correlated aerosol spatial and temporal patterns between satellite measurements and AERONET data. This technique not only successfully extracts the variability of major aerosol regimes but also allows the simultaneous examination of the aerosol variability both spatially and temporally. More importantly, it well accommodates the sparsely distributed AERONET data, for which other spectral decomposition methods, such as Principal Component Analysis, do not yield satisfactory results. The comparison shows overall good agreement between MODIS/MISR and AERONET AOD variability. The correlations between the first three modes of MCA results for both MODIS/AERONET and MISR/AERONET are above 0.8 for the full data set and above 0.75 for the AOD anomaly data. The correlations between MODIS and MISR modes are also quite high (> 0.9). We also examine the extent of spatial agreement between satellite and AERONET AOD data at the selected stations. Some sites with disagreements in the MCA results, such as Kanpur, also have low spatial coherency. This should be associated partly with high AOD spatial variability and partly with uncertainties in satellite retrievals due to the seasonally varying aerosol types and surface properties.

Citation: Li, J., B. E. Carlson, and A. A. Lacis (2014), Application of spectral analysis techniques in the intercomparison of aerosol data. Part II: Using maximum covariance analysis to effectively compare spatiotemporal variability of satellite and AERONET measured aerosol optical depth, *J. Geophys. Res. Atmos.*, *119*, 153–166, doi:10.1002/2013JD020537.

1. Introduction

[2] Aerosols play an important role in the earth's energy budget. Quantifying the radiative effect of aerosols in the climate system requires knowledge of the spatial distribution, temporal evolution, and optical properties of atmospheric aerosols [*Kiehl and Ramanathan*, 2006]. Currently, our understanding of aerosol properties relies heavily on remote sensing measurements from both the space and the surface. Dedicated satellite instruments, such as Moderate Resolution Imaging Spectroradiometer (MODIS) and Multi-angle Imaging Spectroradiometer (MISR), have multispectral designs and sophisticated retrieval algorithms and provide global coverage. Their standard products, including aerosol optical depth (AOD) and Ångström exponent, have been extensively used in scientific research and model validation [e.g., *Kaufman et al*., 2002; *Martonchik et al*., 2009; *Ginoux et al*., 2010; *Petrenko et al*., 2012] and have boosted the rapid progress in aerosol science. Yet satellite retrieval of aerosol properties relies on a series of assumptions such as surface reflectance, aerosol models, and cloud screening [*Martonchik et al*., 2009; *Remer et al*., 2005; *Levy et al*., 2007; *Kokhanovsky et al*., 2007], which all contribute to uncertainties in the retrieved product. Surface measurements using sun photometers make direct measurements of surface radiation and retrieve AOD at higher accuracy. In fact,

This article is a companion to *Li et al.* [2013] doi:10.1002/jgrd.50686 and 10.1002/2013JD020538.

[1]NASA Goddard Institute for Space Studies, New York, New York, USA.
[2]Department of Applied Physics and Applied Math, Columbia University, New York, New York, USA.

Corresponding author: J. Li, NASA Goddard Institute for Space Studies, 2880 Broadway, Room 643 New York, NY 10025, USA. (jl2862@columbia.edu)

2169-897X/14/10.1002/2013JD020537

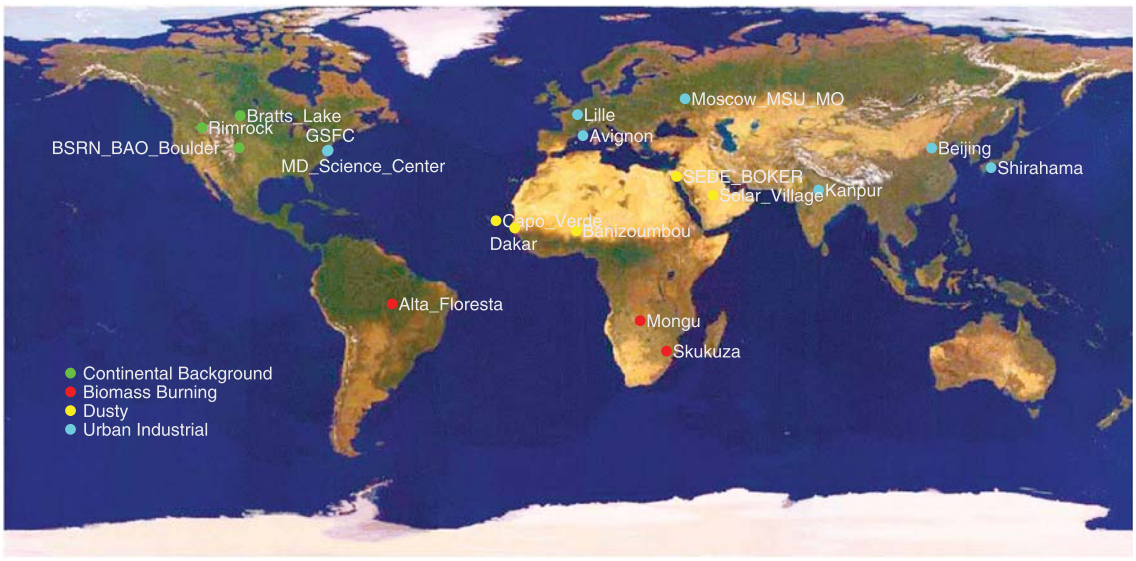

Figure 1. Locations and aerosol types of the selected 20 Aerosol Robotic Network (AERONET) stations. The type information is obtained from *García et al.* [2012].

data from Aerosol Robotic Network (AERONET), a global sun photometer network, are frequently used as ground truth in the validation of satellite retrievals [e.g., *Levy et al.*, 2010; *Kahn et al.*, 2010]. However, one limitation of ground-based data is that these measurements only sample at specific locations and may not be representative of the larger-scale variability that the satellite measures.

[3] In assessing the accuracy of satellite retrievals, the data are usually collocated in space and time with AERONET stations [e.g., *Ichoku et al.*, 2002; *Chu et al.*, 2002; *Abdou et al.*, 2005; *Kahn et al.*, 2005]. Other techniques have been developed to simulate the area that satellites observe by averaging station measurements in time [e.g., *Alexandrov et al.*, 2002a; *Mace et al.*, 2006]. On one hand, these comparisons may overemphasize random measurement noise while neglecting the spatial representativeness of the retrieved quantity. On the other hand, while the accuracy of these instantaneous retrievals is important, many applications, especially those associated with climate forcing and model validation, often rely on the variability at larger temporal and spatial scales (e.g., gridded monthly mean data). For example, many studies aim at resolving the contribution of aerosols in the current climate change by looking at long-term aerosol trends using monthly mean measurements [e.g., *Mishchenko et al.*, 2007; *Kishcha et al.*, 2007; *Kaskaoutis et al.*, 2011; *Yoon et al.*, 2012]. In addition, a recent hot topic involves the interaction between aerosols and climate modes such as the North Atlantic Oscillation [e.g., *Foltz and McPhaden*, 2008; *Evan et al.*, 2009] and El Niño-Southern Oscillation [*Tosca et al.*, 2010; *Li et al.*, 2011] also requires large-scale observations. Moreover, gridded monthly mean products are often of primary interest in validating and constraining aerosol parameterizations used in general circulation models (GCMs), since GCMs typically generate monthly mean outputs [e.g., *Chin et al.*, 2002; *Kinne et al.*, 2006; *Liu et al.*, 2006; *Li et al.*, 2010]. Therefore, it is essential for the available measurements to correctly represent large-scale spatial and temporal aerosol variability.

[4] Spectral decomposition techniques provide effective ways to extract spatial and temporal variability from multidimensional data sets. In Part I [*Li et al.*, 2013], we used empirical orthogonal function (EOF) analysis on four satellite data sets to examine their space-time coherency. We have demonstrated that the analysis successfully extracted major aerosol types and source regions. While the comparison between leading modes indicated overall good agreement across the data sets, some differences still exist and ground-based observations are needed to further investigate the differences and to determine which data set is more reliable in representing certain regions or aerosol types. However, EOF analysis on sparsely sampled surface observations often does not produce satisfactory results, as the variability from each individual station may dominate the global pattern. Maximum covariance analysis (MCA), also known as singular value decomposition (SVD), can be viewed as a generalization of EOF to rectangular cross-covariance matrices between two fields. Since the two data sets are allowed to have different numbers of spatial locations, it is very suitable for comparing satellite with ground observations. Also, since the method maximizes the covariance between two data sets, high variability in individual AERONET stations will be effectively filtered by the better-sampled satellite measurements. Using this technique, we are able to simultaneously compare the spatial distribution and time series of aerosol signals. Another advantage is that the decomposed modes can often be related to aerosol types and physical phenomena. Furthermore, relating observations from a single station to larger-scale satellite data provides insights into the synergy of these two types of measurements, through (1) verifying the accuracy of satellite data using ground observation and (2) extending the spatial representativeness of ground observation using satellite data. Nonetheless, the spatial extension of station data is subject to the accuracy of satellite data and is only rigorous if there is high confidence in the spatial retrieval from the satellite. Meanwhile, it is important to note that this approach does not address any potential bias

Table 1. Moderate Resolution Imaging SpectroRadiometer Dark Target (DT), and Deep Blue (DB) Data Selection at the Aerosol Robotic Network Stations

	JAN	FEB	MAR	APR	MAY	JUN	JUL	AUG	SEP	OCT	NOV	DEC
Alta_Floresta	DT	DT	DT	DT	DT	DT	DT	DT	DT	DT	DT	DT
Avignon	DT	DT	DT	DT	DT	DT	DT	DT	DT	DT	DT	DT
BSRN_BAO_Boulder	DT	DB + DT	DT	DT	DT	DT	DT	DT	DT	DT	DT	DT
Banizoumbou	DB	DB	DB	DB	DB	DB	DB + DT	DB + DT	DB + DT	DB + DT	DB + DT	DB
Beijing	DB + DT	DB + DT	DB + DT	DB + DT	DT	DT	DT	DT	DT	DT	DT	DB + DT
Bratts_Lake	DB + DT	DB	DB + DT	DB + DT	DT	DT	DT	DT	DT	DB + DT	DB + DT	DB + DT
Capo_Verde	DB + DT	DB + DT	DB + DT	DB + DT	DB + DT	DB + DT	DB + DT	DB + DT	DB + DT	DB + DT	DB + DT	DB + DT
Dakar	DB + DT	DB + DT	DB + DT	DB + DT	DB + DT	DB + DT	DB + DT	DB + DT	DB + DT	DB + DT	DB + DT	DB + DT
GSFC	DT	DT	DT	DT	DT	DT	DT	DT	DT	DT	DT	DT
Kanpur	DT	DT	DT	DB + DT	DB	DB	DB + DT	DT	DT	DT	DT	DT
Lille	DT	DT	DT	DT	DT	DT	DT	DT	DT	DT	DT	DT
MD_Science_Center	DT	DT	DT	DT	DT	DT	DT	DT	DT	DT	DT	DT
Mongu	DT	DT	DT	DT	DT	DT	DT	DT	DT	DT	DT	DT
Moscow_MSU_MO	DB + DT	DB + DT	DT	DT	DT	DT	DT	DT	DT	DT	DT	DB + DT
Rimrock	DT	DT	DT	DT	DT	DT	DT	DT	DT	DT	DT	DT
SEDE_BOKER	DB	DB	DB	DB	DB	DB	DB	DB	DB	DB	DB	DB
Shirahama	DT	DT	DT	DT	DT	DT	DT	DT	DT	DT	DT	DT
Skukuza	DT	DT	DT	DT	DT	DT	DT	DT	DT	DT	DT	DT
Solar_Village	DB	DB	DB	DB	DB	DB	DB	DB	DB	DB	DB	DB

between the data sets, but rather provides a quantitative evaluation of the space-time variability of the measurements. However, since it is this variability that defines the trends and changes in physical processes that alter the AOD, this technique provides a powerful tool with which to examine whether the satellite and correlative ground-based measurements agree on AOD variability.

[5] In this paper, we present comparison between satellite retrievals of AOD from Aqua-MODIS and MISR, and AERONET data using the MCA method. The Terra-MODIS data is not used here mainly because its deep blue product that covers the desert regions is not as complete as Aqua-MODIS. To our knowledge, this is the first study applying this technique to aerosol measurements and data comparison. Our results indicate an overall good agreement between satellite and AERONET measured AOD and verify many documented phenomena, which confirms the usefulness of this method in comparing spatiotemporal variability. Section 2 describes the data sets used in the study. Section 3 gives a detailed description of the method and the analysis procedure. The results are presented in section 4. In section 5, we further discuss the spatial representativeness of the AERONET stations. The conclusions are summarized in section 6.

2. Data

2.1. AERONET Sun Photometer Data

[6] Direct measurements from the AErosol RObotic NETwork (AERONET) [*Holben et al*., 1998] are usually considered as ground truth when assessing satellite retrievals of aerosol properties. The uncertainty of AOD retrieval is reported to be 0.01 at the visible and near IR wavelengths and increases to 0.02 in the UV [*Eck et al*., 1999]. This study uses AERONET Level 2 quality assured and cloud screened [*Smirnov et al*., 2000] monthly mean AOD data from 19 carefully selected stations. Because the MCA analysis requires the construction of the temporal covariance matrix, the primary selection criterion is the length and completeness of data records. The qualified stations preferably have less than 10 missing months from January 2003 to December 2011. However, four stations: Beijing, Capo_Verde, Dakar, and Mongu, which do not strictly meet the above criterion, are manually added to account for major aerosol regimes. Figure 1 shows the locations of the selected AERONET stations and their aerosol types. The spatial distribution of these stations covers four major aerosol regimes: dust, biomass burning, urban industrial, and continental background. The determination of the aerosol type at each station is based on *García et al*. [2012]. Nonetheless, because our selection criterion places emphasis on temporal sampling at the expense of spatial coverage, the selected stations are limited and not all aerosol source regions and types are represented.

[7] For effective comparison with satellite data, the AERONET AOD are converted to 550 nm using measurements from 380 nm to 870 nm by applying a second-order polynomial fitting of ln (AOD) vs. ln (wavelength) [*Eck et al*., 1999]. Also, despite the strict selection, several stations still have missing data for certain months. These gaps are filled using the multiyear averaged value for that month at that station, so that the interpolated data should have minimal influence on both the seasonal and interannual variability.

2.2. Satellite Data

[8] In this study, we focus on Level 3 gridded monthly mean AOD data from MODIS onboard the EOS-Aqua platform and MISR onboard the EOS-Terra platform, for the time period from January 2003 to December 2011.

[9] The MODIS instrument is a single-view imager with a swath width of 2330 km and near global coverage of 2 days. This high sampling frequency captures most of aerosol variability and microphysics properties. The AOD data used here belong to Collection 051, available from ftp://ladsweb.nasacom.nasa.gov/allData/51/MYD08_M3. The data resolution is 1° × 1°. We select the QA weighted averages (variables named "*QA_Mean_Mean"), i.e., data with higher QA values are given larger weights in the averaging [*Hubanks et al*., 2008]. To ensure global coverage, we combine ocean, dark target [*Levy et al*., 2010; *Remer et al*., 2008], and deep blue retrievals [*Hsu et al*., 2004, 2006] at 550 nm. The combination of dark target (DT) and deep blue (DB) over land uses the scheme by *Levy et al*. [2013], which uses monthly Normalized Difference Vegetation Index (NDVI) climatology from MODIS land product as a mask to select the algorithm. Specifically, if NDVI > 0.3, DT is used. If NDVI < 0.2, DB is used. And if NDVI lies in between, a simple average of DT and DB is used. Note that due to the seasonal variation of surface vegetation, there may be seasonal changes in the data selected for some AERONET stations. Table 1 lists the data selected for each station. The MODIS cloud screening scheme takes advantage of the different spatial variability of clouds and aerosols [*Martins et al*., 2002] along with tests of brightness in visible and infrared channels. We are aware that previous studies suggested that cloud contamination may still remain in the quality assured MODIS product and have developed correction methods to eliminate the incorrectly cloud screened data [e.g., *Zhang and Reid*, 2006; *Hyer et al*., 2011]. However, their filtering will eliminate more than half of the data volume and since spatial coverage is important in our analysis we examined the data for any obvious dependence on cloud fraction.

[10] This analysis did not reveal any obvious dependence of MODIS/AERONET AOD difference on cloud fraction, on the monthly mean scale (Figure not shown). Therefore, we retain the standard Level 3 product in our analysis without further filtering. In using spatially and temporally averaged data such as Level 3 AOD, there is a question whether different averaging schemes may introduce sporadic differences in the final result. As pointed out by *Levy et al*. [2009], global mean AOD may vary by as much as 30% simply due to the way the measurements are aggregated. We have tested the effects of four different averaging schemes: straight average, pixel threshold, pixel weighted, and pixel threshold weighted averaged as described in *Levy et al*. [2009] by comparing the analysis results with the QA weighted average and find that the MCA decomposition results are not sensitive to the details of the aggregation scheme (figures not shown).

[11] The MISR instrument has nine pushbroom cameras. The zonal overlap of the common swath of all nine cameras is at least 360 km in order to provide multi-angle coverage in 9 days at the equator and 2 days at the poles [*Diner et al*., 1998]. Compared to the dark target MODIS algorithm, the multi-angle view of MISR has better capability over bright surfaces [*Abdou et al*., 2005; *Kahn et al*., 2009]; however, its lower sampling may not fully resolve small-scale variability. In this study we use version 31 Level 3 gridded monthly products of the green band (555 nm), available from http://eosweb.larc.nasa.gov. The original 0.5° × 0.5° data resolution has been downgraded to 1° × 1°. The rescaling is performed by assigning equal weights to each subgrid, and the final 1° × 1° grid is considered valid only when more than half of the subgrids have valid data.

[12] MODIS and MISR have different sampling frequencies due to their different instrumental design. In addition, MODIS and MISR also use different aerosol models, surface parameterization, and cloud screening to retrieve aerosol properties. In this study, we will demonstrate that despite these differences, both data sets agree well with ground truth in terms of spatiotemporal variability.

3. Method

[13] Maximum covariance analysis (a.k.a. SVD analysis, *Bretherton et al*., 1992; *Björnsson and Venegas*, 1997) aims at finding the coupled modes of two data fields by singular value decomposition of their cross-covariance matrix. Similar to EOF analysis, this is a dimensional reduction technique, as the leading modes with largest singular values can recover most of the variance in the two high dimensional data sets. In addition, considering two high dimensional data sets X and Y, each pair of mode x_i and y_i will have the following properties: (1) maximizing covariance implies that the leadings x_i and y_i have reasonably high correlation and each describes a large fraction of the variance in X and Y, respectively; (2) x_i is correlated with y_i but is orthogonal to other modes of Y; (3) each x_i is also orthogonal to the other modes of X, and the same for each y_i. The method has been commonly applied to observations of two different variables, such as sea surface temperature and sea level pressure. Here we demonstrate that it is also useful in comparing two different measurements of the same variable. The detailed procedure is described as follows:

[14] Assuming two data matrices X and Y. X is satellite data of dimension $N \times P$ (N time measurements at P grid boxes) and Y is the ground observation of dimension $N \times Q$ (N time measurements at Q locations). After removing the mean from each time series in X and Y, we begin by constructing the cross-covariance matrix

$$C = X^T Y$$

[15] Performing SVD on C

$$C = U \Sigma V^T$$

[16] U and V are orthogonal matrices whose columns are singular vectors for X and Y, respectively, and each pair of singular vectors represents covarying modes between X and Y. The time series A and B describing how each mode oscillates in time are then found by

$$A = XU$$
$$B = YV$$

[17] The diagonal matrix $\sum$ contains singular values in descending order. Let σ_i denote the i-th element of $\sum$; the fraction

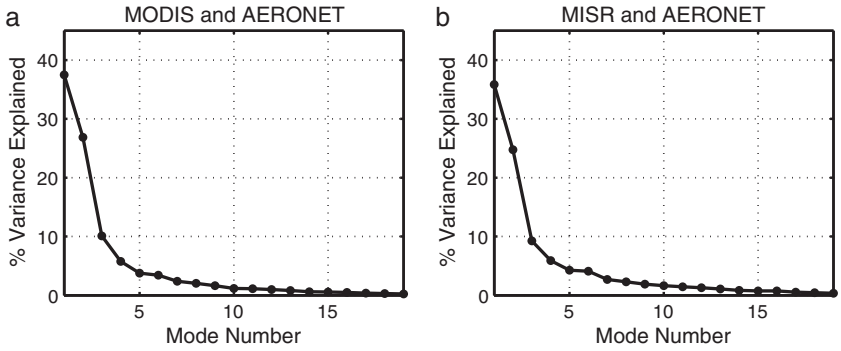

Figure 2. Variance explained by the maximum covariance analysis (MCA) modes for (a) Moderate Resolution Imaging SpectroRadiometer (MODIS) and AERONET and (b) Multi-angle Imaging SpectroRadiometer (MISR) and AERONET, decomposed using the full data sets.

of squared covariance (*SCF*) explained by the *i*-th mode is given by

$$SCF = \frac{\sigma^2{}_i}{\sum_{j=1}^{N} \sigma^2{}_j}$$

[18] The first mode of MCA maximizes the covariance between the two data sets, the second mode maximizes the remaining covariance, and so on. In this way, the coherency of the two measurements is effectively examined by the degree of agreement or correlation between the spatial patterns and time series of the leading modes.

[19] Moreover, because monthly mean aerosol variability is usually dominated by strong seasonal cycles, we also perform MCA on the anomaly data constructed by removing the multiyear averaged seasonal cycle. This analysis further isolates aerosol source regions and extracts interannual variability.

4. Results

[20] This section presents MCA results of the full MODIS/MISR and AERONET data sets, which are dominated by strong seasonal variability, as well as the anomaly data, which allow us to compare interannual variability.

[21] The number of MCA modes to examine is primarily determined by the behavior of the variances explained by each mode, which is shown in Figure 2. From Figure 2, we are able to observe that for both MODIS and MISR, the variance dropped from above 10% at Mode 3 to ~5% at Mode 4. Also, the first three modes account for ~70% of the total variance. Therefore, we focus our discussion on the first three modes, which are presented in Figure 3. Mode 1 and Mode 2 both exhibit seasonal cycles, while the third mode indicates semi-annual variability. From Figure 3, it is clearly seen that both satellite data sets agree well with AERONET in terms of the spatial pattern and time series. The correlations between the satellite and AERONET time series for all three modes are well above 0.75, and the distribution of their spatial signals is almost identical with only few exceptions. The patterns between MODIS/AERONET and MISR/AERONET are also quite similar, indicating coherency across the three data sets. PC 1–3 of MODIS modes (Figure 3a) and MISR modes (Figure 3b) are highly correlated at 0.99, 0.98, and 0.99, respectively. The variances explained by MISR/AERONET modes are comparatively lower because the narrower swath and longer revisit time of MISR tend to reduce the temporal representativeness of its data and lead to the higher noise ratio.

[22] The MCA patterns and time series of the satellite data are similar to the EOF analysis of each individual field presented by *Li et al*. [2013]. The seasonality represented by Mode 1 should correspond to the aerosol variability primarily controlled by meteorological conditions (wind and precipitation, etc.) for the Northern Hemisphere (NH). The positive signals for the NH in Mode 1 mainly come from dust-dominated regions of North Africa, Arabian Peninsular, and Central Asia, and industrial pollution and its transport from North India, Northeast Asia, and North Pacific. The aerosol loading for these regions peaks in late spring to summer, in phase with PC 1. The second mode captures aerosol variability for the Southern Hemisphere (SH), highlighting biomass burning aerosols from South America, South Africa, and Southeast Asia. Note that the Sahel region also appears in Mode 2 but as a negative feature. This region is primarily dominated by dust with seasonal biomass burning activities. The aerosol loading peaks during the winter months of December to February, which is out of phase with the SH biomass burning regions which peak during the August to October months [*Ducan et al*., 2003]. Mode 3 captures two regions affected by mixed aerosol types showing different seasonal variations: Northern India and the Sahel. The Northern India AOD is dominated by dust during premonsoon and monsoon seasons [*Dey et al*., 2004] and anthropogenic aerosols during the postmonsoon and winter seasons [*Singh et al*., 2004]. The Sahel AOD has a primary peak in the summer influenced by dust from North Africa and a secondary peak in the winter due to dust and some biomass burning. In addition, some signals of biomass burning aerosols from Southeast Asia and South America are also present in this mode. The peak biomass burning season for Southeast Asia is from February to April, and that from South America is from August to October [*Duncan et al*., 2003]. The annual cycle of PC 3 exhibits two peaks during these two seasons, respectively. Therefore, it projects on the spatial pattern as positive signals over these two regions.

[23] The above good agreement between both satellite data sets and AERONET is encouraging. However, it is also worth noting the differences between the satellite and AERONET data, as well as those between MODIS and MISR, although they are not particularly significant. For example, North India

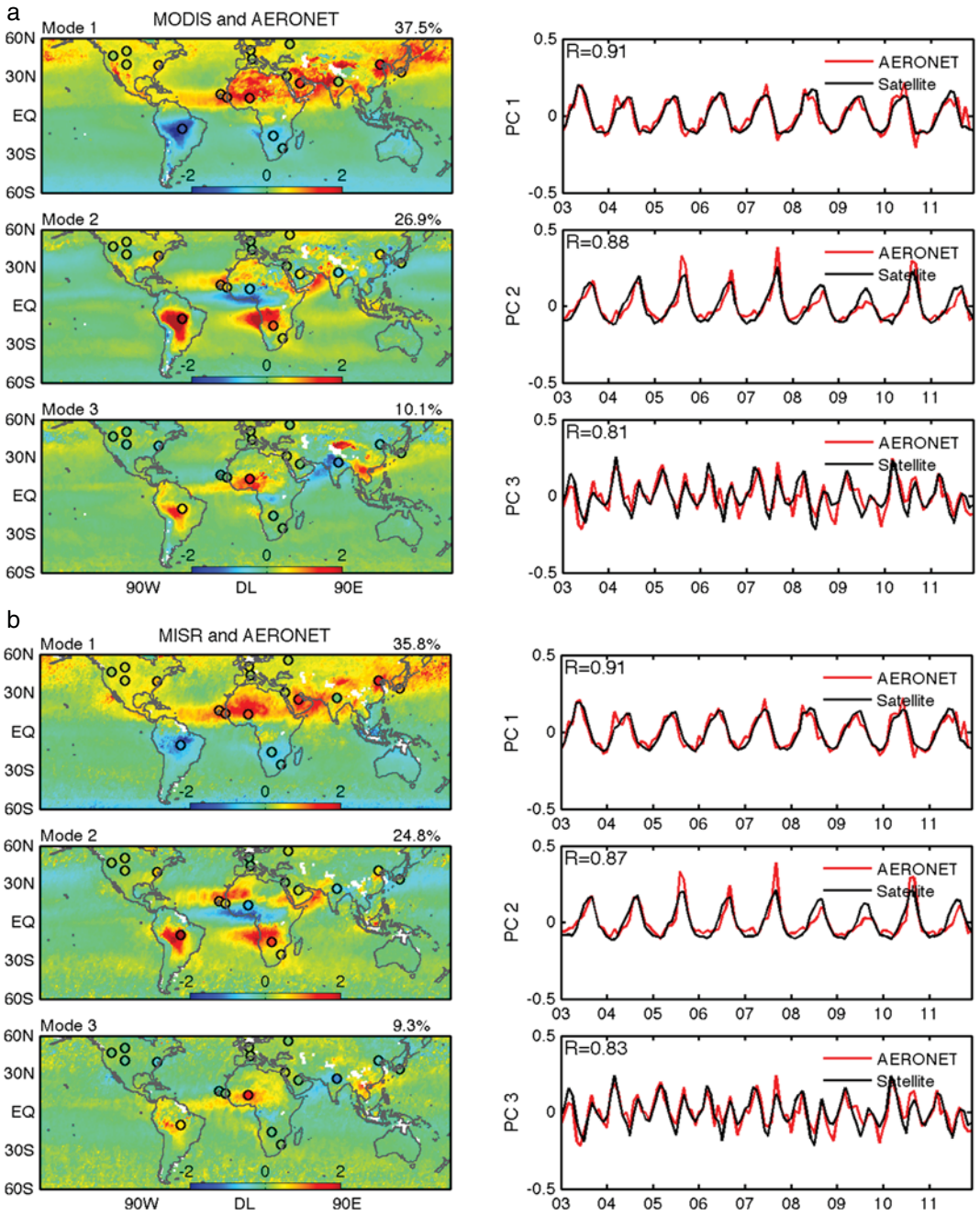

Figure 3. The spatial pattern and time series of the first three modes for (a) MODIS/AERONET and (b) MISR/AERONET, decomposed from the full data set. Spatial distribution of the AERONET results is superimposed on each satellite map with the same color scale. The number in the upper right corner of each spatial map shows the variance explained by this mode and the *R* values in the upper left corner of the time series plots are the correlation coefficients between the two time series. The red colors on the spatial maps indicate regions where aerosol optical depth (AOD) varies in phase with the PC time series, while the blue colors indicate regions where AOD varies out of phase with the PC.

is a typical region where neither MODIS nor MISR agree well with AERONET in Modes 1 and 2. This region has highly varying surface properties and changing aerosol species with season. Previous studies have found that the MODIS retrievals tend to overestimate AOD during premonsoon and monsoon seasons while it underestimates AOD during postmonsoon and winter seasons [*Tripathi et al*., 2005; *Jethva et al*., 2007]. *Levy et al*. [2010] also indicated that bias in the assumed aerosol single scattering albedo results in the error of MODIS AOD over this area. The overestimation of MODIS during the dust season may lead to its the stronger variability over North India in Mode 1, while its underestimation during the winter months may result in its weaker signal in Mode 2 for this region. The performance of MISR over North India is slightly better for Modes 1 and 2. This should be partly attributed to its multi-angle design that makes use of directional surface

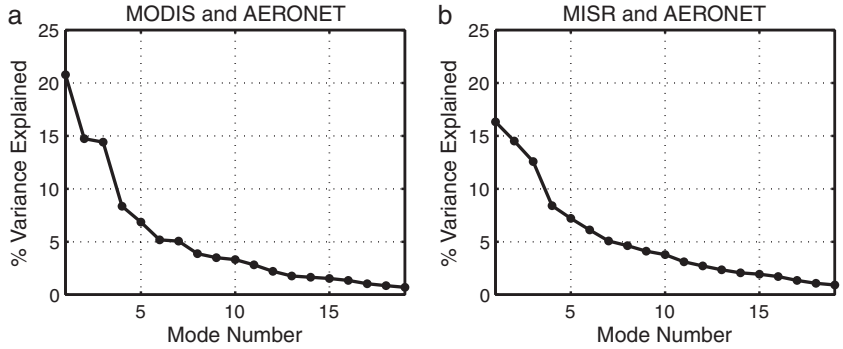

Figure 4. Variance explained by the MCA modes for (a) MODIS and AERONET and (b) MISR and AERONET, decomposed using the deseasonalized data sets.

properties [*Martonchik et al*., 2004; *Prasad and Singh*, 2007]. In addition to the above reasons, as we note in section 5, some of the differences observed for North India may result from the high spatial variability of aerosol properties and thus low spatial representativeness of the AOD over this area. Another difference between the spatial patterns of MODIS/AERONET and MISR/AERONET is that the MISR signal over South America is weaker in all three modes of Figure 3. Previously, *Kahn et al*. [2009] and *Shi et al*. [2011] pointed out that the underestimation of MISR over this region is possibly attributed to different cloud screening methodologies, where MISR might have screened out heavy smoke conditions as cloud. The low variability identified in the PCs also likely results from MISR's conservative cloud screening.

[24] In summary, the MCA validates satellite data in capturing the correct spatial and temporal variability of the AOD through comparison with ground-based AERONET data and the general agreement between the satellite data sets, suggesting that it can provide information on most aerosol processes. It also helps to extend station observations to a larger regional scale. Many previously documented disagreements are also identified through this analysis. These results suggest that MCA is an effective way to simultaneously compare the spatial and temporal variability in two different data sets with a focus on the modes that account for most of the observed variance in both fields.

[25] Next, we go on to the examination of interannual variability using AOD anomaly data. We again determine the number of significant modes to be three based on the large falloff in the amount of the variance explained from Mode 3 to Mode 4 (Figure 4). The first three MCA modes of anomaly data are shown in Figure 5. Because the bulk of the AOD signal comes from seasonal variability, the noise level is higher in the deseasonalized data. As a result, the fraction of squared covariance explained by the dominant modes in Figure 5 is significantly lower than those shown in Figure 3. The first three modes account for ~50% of the total variance. Despite the noise, the spatial and temporal patterns between satellite and AERONET still agree well. The spatial patterns appear more isolated showing aerosol source regions separately, and the corresponding time series captures their interannual variability.

[26] Mode 1 in Figure 5 of both data pairs is clearly associated with biomass burning aerosols over central South America. The PC of this mode has strong peaks in September and exhibits strong interannual variability. The positive anomaly in 2007, followed by two negative anomalies in 2008 and 2009, is consistent with *Torres et al*. [2010]. The 2010 positive anomaly is likely triggered by the dry condition and is consistent with CO measurements from *Hooghiemstra et al*. [2012]. The second Mode has a positive signal over Northeast Asia and North Pacific. This region is primarily dominated by urban industrial aerosols that peak in the summer, with periodic intrusions of dust in the spring to early summer [*Xin et al*., 2007; *Yu et al*., 2009]. This time series shows a continuous increasing trend from 2004 to 2007, which is in line with the previously reported aerosol increase or surface dimming over East Asia [e.g., *Wang et al*., 2009; *Lu et al*., 2010]. The short-term reduction in 2008 might be attributed to air quality control measures during the Olympic games [*Wang et al*., 2010; *Guo et al*., 2013] and meteorological conditions [*Cermak and Knutti*, 2009; *Gao et al*., 2011]. Nonetheless, the study time period is still too short to represent any long-term trends. The third mode appears to be associated with dust emission over North West Africa and its transport to the North Atlantic. The strong peak in spring 2010 should correspond to the unusual dust outbreak in that year [*Jung et al*., 2013]. Also, consistent with Figure 3, the first three modes for MODIS and MISR also agree well in terms of spatial and temporal variability. The correlations between PC 1 and 3 for the MODIS and MISR results are 0.94, 0.87, and 0.94, respectively.

[27] Finally, the spatial signals in the MISR AOD data are, in general, weaker than those in both the AERONET and MODIS AOD date. On one hand, many of the isolated regions have been found to have comparatively large MISR-MODIS discrepancy [*Kahn et al*., 2009, 2010], which is confirmed by the MCA results. On the other hand, due to the narrower swath of MISR, many of its monthly mean products are averaged from only three to four daily samples. Therefore, the signals in the MISR anomalies are more likely to be contaminated by the noise in the measurements. This raises the question of the temporal representativeness of the measured quantity, which will be the subject of future study. Nonetheless, the overall agreement increases our confidence in using satellite data to study the large-scale interannual variability of major aerosol types and source regions.

5. Discussion

[28] Section 4 presents the results showing good agreement in the large-scale variability of the MCA modes, but

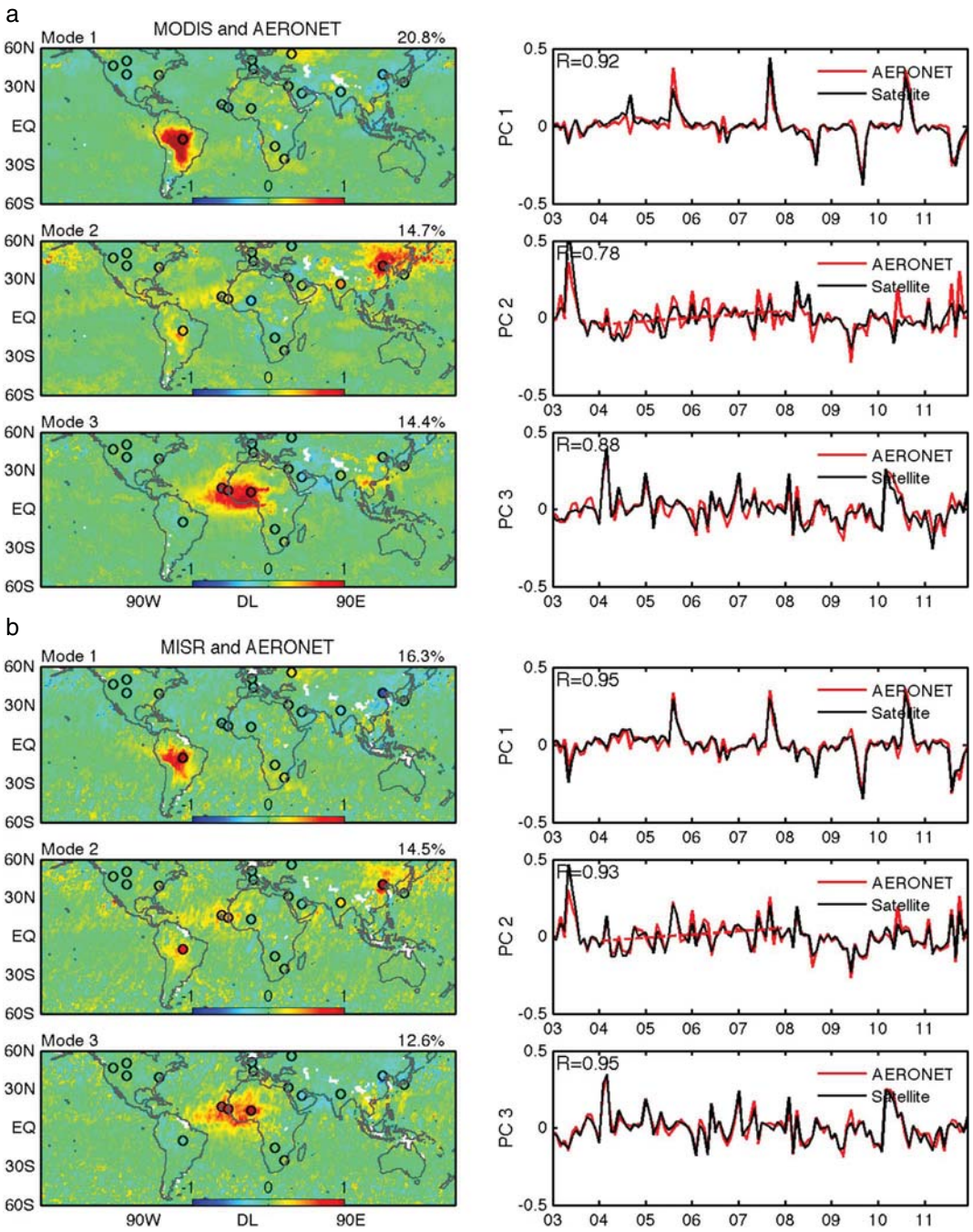

Figure 5. The first three MCA modes for the deseasonalized AOD data for (a) MODIS/AERONET and (b) MISR/AERONET, with AERONET results superimposed. Satellite and AERONET data still agree well in the deseasonalized modes. The first mode represents interannual variability of South America biomass burning, the second shows pollution and dust around Beijing, and the third captures dust emission and transport from North West Africa. The red dashed line in the time series of Mode 2 shows the linear regression trends from 2004 to 2007.

also reveals places with disagreements. Unlike satellite observations that have extensive spatial coverage, ground measurements only sample at a specific location. Therefore, the spatial representativeness of AOD at the AERONET stations, which reflects local variability, may also contribute to the differences between the MCA modes of the satellite and AERONET data. In this section, we examine the spatial representativeness of AOD at each AERONET site in order to provide further insights into the interpretation of the MCA results. It is important to note that the "spatial representativeness" does not refer to any specific AERONET station, but rather to the AOD parameter, i.e., the degree of AOD spatial variability around the station. As regions affected by similar aerosol types or transport mechanisms will have correlated time series of aerosol properties, the spatial range of the correlated region is closely related to the scale of aerosol variability and can serve

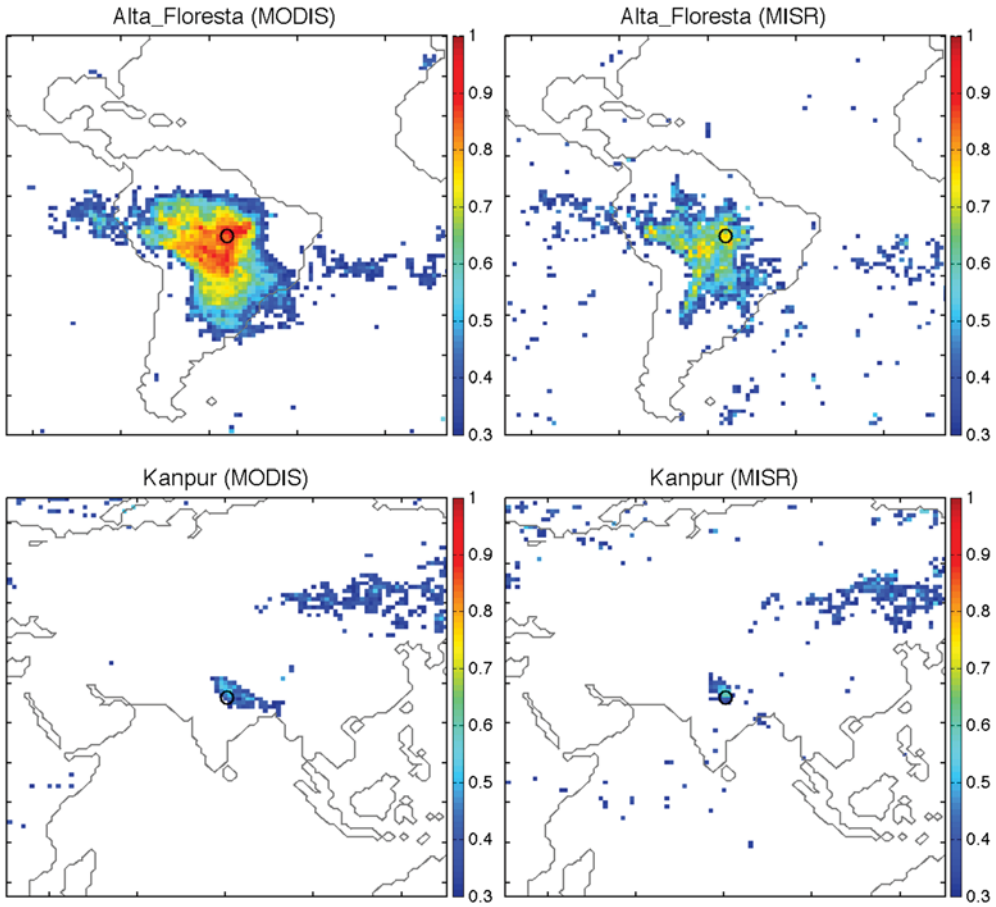

Figure 6. The spatial representativeness of AOD measurement at two typical stations: Alta_Floresta and Kanpur. The representativeness is good at Alta_Floresta, with both higher correlation and larger area than Kanpur. The low representativeness at Kanpur may be due to both high AOD variability and satellite retrieval uncertainties and may partly contribute to the disagreement between the MCA Mode 1 of Figure 3. The MISR result is noisier due to its low sampling frequency, which is illustrated in Figure 7.

as a proxy for the representativeness. Therefore, we take a simple approach by calculating the correlation between the AOD anomaly time series of each AERONET station and that of all satellite grid boxes and screening the correlation coefficients by a threshold of 0.3 and p-value of 0.01. In this way, the area of satellite data that is highly correlated with the ground station is considered to be well represented by the AOD measurement at that station. A similar approach has been implemented by previous studies such as *Hoelzemann et al.* [2009] to investigate the representativeness of AERONET measurements in South America.

[29] In Figure 6, we show two typical stations with good (Alta_Floresta) and poor (Kanpur) representativeness, respectively, for MODIS and MISR. For Alta_Floresta, the satellite data over a large area around that station are highly correlated with AERONET measurement. The correlation in general decreases with distance, which is an indication of aerosol source and transport structure. The spatial correlation pattern for Alta_Floresta agrees well with *Hoelzemann et al.* [2009] results for area with correlation > 0.5. Some differences from *Hoelzemann et al.* [2009] may be associated with differences in record length and study period (*Hoelzemann et al.*

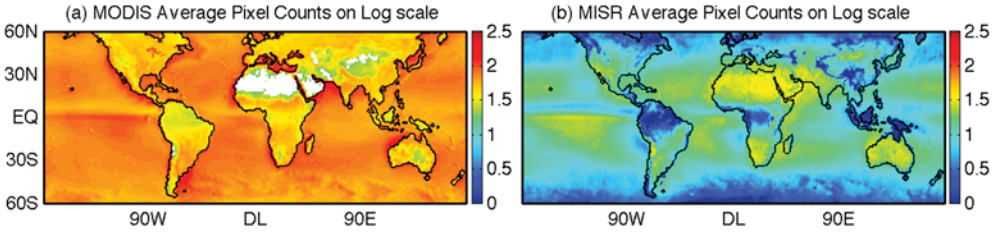

Figure 7. Averaged monthly mean pixel count map for (a) MODIS and (b) MISR for the study period on log scale. The pixel count information is not available for MODIS Level 3 deep blue product. MODIS has significantly more samples for each grid box than MISR due to its wider swath and thus shorter revisit time.

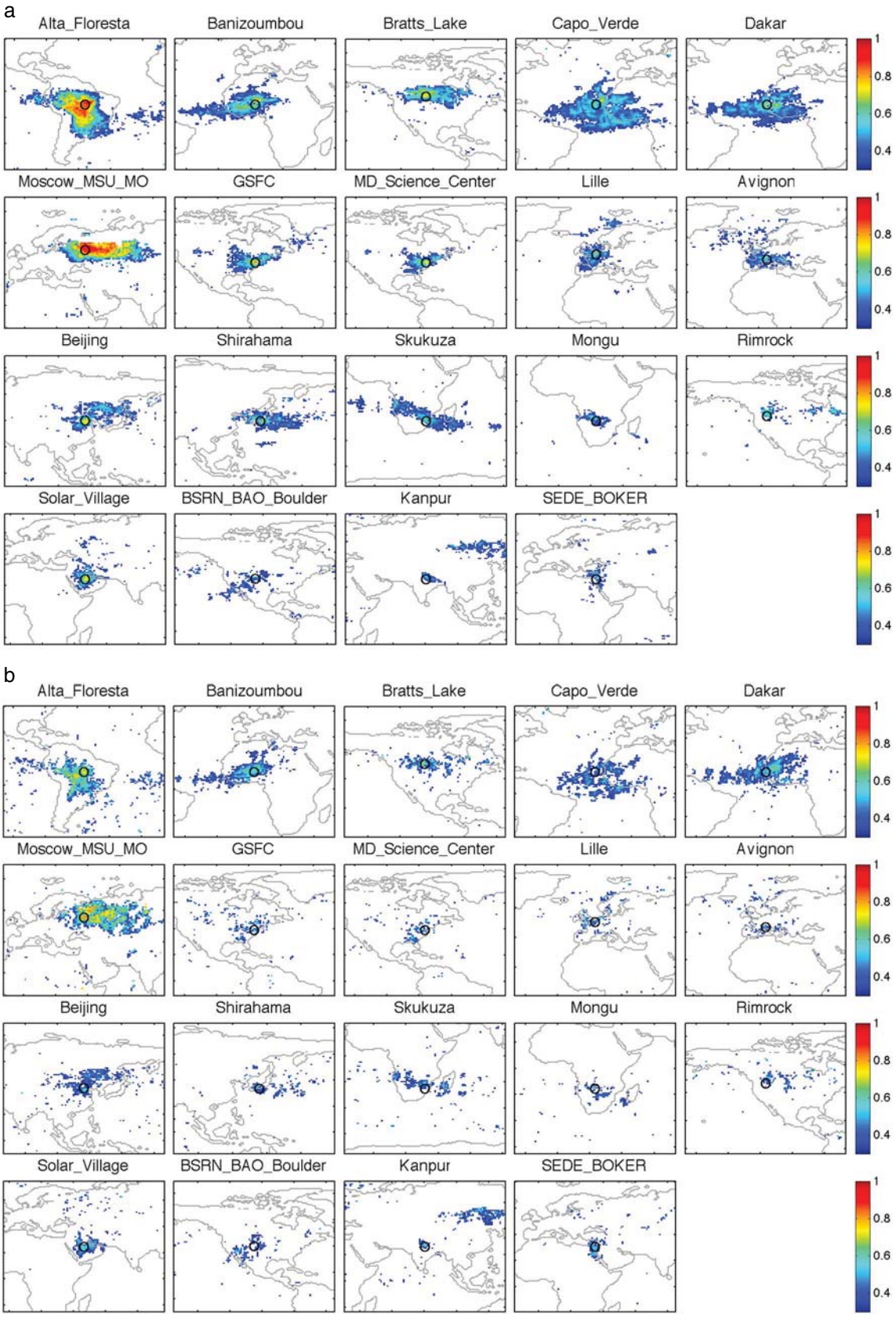

Figure 8. Spatial representativeness of AOD at all the selected AERONET stations calculated using (a) MODIS AOD data and (b) MISR AOD data. The majority of the stations have high to moderate representativeness. These stations also show good agreement in the MCA modes.

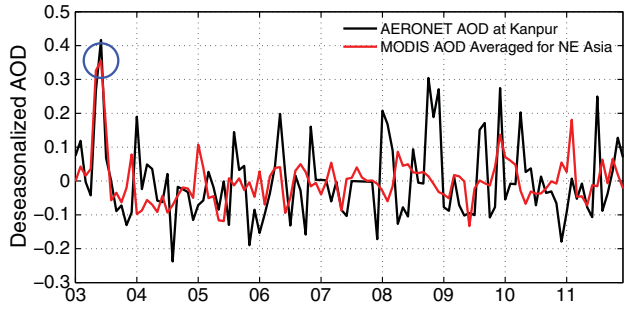

Figure 9. Time series of AERONET AOD at Kanpur and MODIS AOD averaged over the Northeast Asia regions that have correlations with Kanpur. The coherent strong peak in 2003 is responsible for the correlation between Kanpur and Northeast Asia shown in Figure 8. The correlation between the two time series from 2004 to 2011 is 0.025.

used only biomass burning seasons from 2001 to 2007 while the whole time series from 2003 to 2011 is considered here). This good spatial agreement between MODIS and AERONET at Alta_Floresta should be attributed to two factors: (1) aerosol type does not vary significantly with season in this part of Amazonia; (2) there is little regional topographic variation or barriers to meteorological transport of aerosols. In contrast, the data at Kanpur station is only correlated with MODIS and MISR for the narrow region of the Indo Gangetic Plain, and the degree of correlation is also much lower. The low AOD representativeness at Kanpur may be attributed to two factors: (1) The aerosol types are highly variable, with coarse mode dust dominating in the spring, fine mode pollution and biomass burning aerosols dominating in the winter, and mixtures of fine and coarse mode during other months [*Eck et al.*, 2010]. Regional topography is also complicated with mountains establishing natural barriers to aerosol transport. This complexity results in the highly variable spatial distribution of aerosol properties, and measurements at a single point cannot fully resolve the variability of the whole area. (2) The varying aerosol types and topography result in seasonal variation in aerosol absorption and size distribution, as well as surface reflectance. All of these factors tend to introduce large uncertainty to satellite retrievals and thus lead to the low correlation between AERONET and satellite data. Both the high AOD variability (representation error) and uncertainties in the satellite retrievals (measurement error) help to explain the poor agreement in Mode 1 and Mode 2 of the MCA results between satellite and AERONET for Kanpur. However, the contribution of these two error sources will be analyzed and addressed in a separate study. Also, note in Figure 6 that MISR appears to have noisier spatial patterns and lower correlations than MODIS. This is mainly attributed to its longer revisit time, which leads to fewer samples in the MISR monthly means. Therefore, its signal tends to have a greater noise contribution from instantaneous measurements. Figure 7 shows the averaged pixel count map for MODIS and MISR monthly mean data over the study period. It is clear that with its wider swath, overall MODIS has significantly more samples for each grid. Nonetheless, the spatial patterns of MISR MCA modes agree well with AERONET in spite of its low sampling frequency. This result well demonstrates the usefulness of this method in extracting signal and reducing noise.

[30] Figure 8 shows the representativeness of all the selected AERONET stations. Focusing on the MODIS maps, most stations over Northwest Africa, North America, South America, and Europe have good representativeness, with both high correlation and wide coverage. The representativeness of Asian and South African stations is also reasonable. Note that the representativeness at Mongu is lower than that at a nearby station — Skukuza. This may be again partly due to uncertainties in satellite retrievals. As pointed out by *Eck et al.* [2013], Mongu has seasonally varying aerosol single scattering albedo while the MODIS retrieval assumes a constant single scattering albedo. These are also places with good MCA agreements. Moreover, the spatial representativeness of several stations, such as Alta_Floresta, Banizoumbou, Capo_Verde, Dakar, Beijing, and Mongu, are similar to the MCA patterns around these areas, which further confirms that the MCA modes capture regionally coherent aerosol processes. In addition to Kanpur, low representativeness is also found for SEDE_BOKER. However, this station only has weak signals in the global MCA modes and a closer comparison will require regional analysis.

[31] Meanwhile, it is also important to point out that the correlation analysis of spatial representativeness may introduce spurious correlations at far away locations due to coherent events or limited sample size. For example, the Kanpur station appears to be moderately correlated with some area in Northeast Asia. Further examining the time series of AERONET at Kanpur and averaged MODIS AOD over the correlated region in Northeast Asia, we find that this positive correlation is primarily caused by the strong peak in spring 2003 (Figure 9). The correlation between the two time series from 2004 to 2011 sharply decreases to 0.025. In addition, measurements at a few stations, including Solar_Village and SEDE_BOKER, show correlation with some high latitude regions. This could be partly due to missing satellite observations during polar nights and partly associated with limited temporal sampling (180 month) so that a few coherent data points significantly affect the correlation. Measurement at Rimrock station also appears to be correlated with far away places of Quebec, Canada. Comparison between the

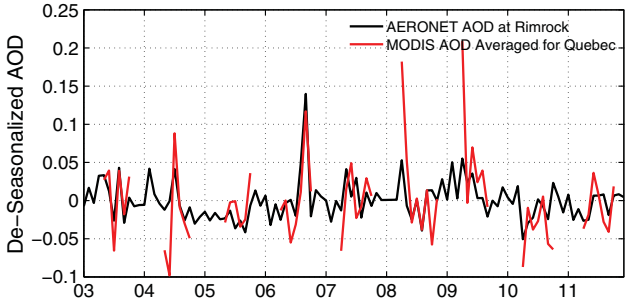

Figure 10. Time series of AERONET AOD at Rimrock and MODIS AOD averaged over the Quebec region that is correlated with Rimrock. The lack of sampling of MODIS data during winter and coincident agreements during some summer months results in the spurious correlation between these two remote locations.

AERONET AOD time series at Rimrock and MODIS AOD averaged over the Quebec region (black box in the Rimrock panel of Figure 8), as shown in Figure 10. We can see that Quebec region usually lacks satellite measurements during the winter months. Some coincident agreements between MODIS and AERONET AOD during the summer months, especially the two peaks in 2004 and 2006, result in the spurious correlation. This sampling-related spurious correlation is a common issue in the construction of background covariance matrix using ensembles for data assimilation and various localization techniques have been developed to mitigate this problem [e.g., *Evensen*, 2003; *Buehner and Charron*, 2007; *Bishop and Hodyss*, 2009]. However, investigation of localization methods is beyond the scope of the current study and the readers should focus on the region surrounding the station in interpreting the representativeness results. Finally, it should be noted that the AERONET representativeness considered here only refers to a space dimension larger than $1° \times 1°$ scale, for the purpose of facilitating the interpretation of MCA results. In a different study, we will perform a more extensive examination of both spatial and temporal representativeness at a variety of scales.

6. Conclusion

[32] In this study, we introduce the MCA method as an effective way to examine the spatiotemporal coherency between satellite and ground observations of aerosol optical depth. The major advantages of this approach include: (1) verifying satellite data by finding the correlated modes with ground observation, and these modes also represent most of the variance in each individual field; (2) relating the comparison to aerosol types, sources, and physical phenomena.

[33] The comparison between the spatial pattern and time series confirms that satellite data well represent the seasonal variability of dust over North Africa, Central and East Asia, biomass burning over South America, South Africa, Southeast Asia, and the Sahel. The interannual variability for these aerosol regimes, as well as urban aerosols over East Asia and North India, is also captured by MCA modes of the deseasonalized AOD. Moreover, the results also reflect areas that have previously been identified as problematic in satellite retrievals, including the Kanpur site for MODIS, and South America for MISR.

[34] To help interpret the MCA results, we also investigate the spatial representativeness of the AOD measurement at the AERONET stations by correlating the time series at each site with all satellite grid boxes. It is encouraging that the majority of the stations have moderate to high representativeness. The similarity between the distribution of representative area and MCA spatial pattern further confirms the validity of the MCA technique. The lower spatiotemporal coherency between AERONET and satellite data at some stations, such as Kanpur, could be attributed to high AOD spatial variability, as well as uncertainties in the satellite retrievals.

[35] The MCA method is easily extended to the comparison of other data sets or variables. And in addition to its usage in incorporating sparse ground observations, there is no doubt that it can be applied to two satellite data sets. Finally, the results presented here do not provide information on aerosol variability in all regions. Our future work will involve a comprehensive intercomparison study using other available aerosol retrievals but relaxing the temporal completeness criterion to more completely assess the spatial representativeness of the data and identify where the satellite retrievals have problems. For example, Europe and North America do not show up in the leading modes due to their relatively small aerosol loading. Detailed study of these regions will require localized analysis. The MCA can also be applied to other aerosol parameters such as the Ångström exponent (AE). Although the AE products are generally less reliable, it is useful in constraining aerosol size parameterization in GCMs and the monthly mean data will be less noisy. Comparison could also be made between radiance measurements for specific aerosol regions or scenes, as these invoke fewer assumptions.

[36] **Acknowledgments.** We thank the MODIS, MISR, and AERONET science team for providing the data used in this research. We also thank the anonymous reviews for providing helpful comments and suggestions in improving the manuscript. This study is funded by NASA climate grant 509496.02.08.04.24. Jing Li is funded by the NASA Postdoctoral Program (NPP), administrated by the Oak Ridge Associated Universities.

References

Abdou, W. A., D. J. Diner, J. V. Martonchik, C. J. Bruegge, R. A. Kahn, B. J. Gaitley, K. A. Crean, L. A. Remer, and B. Holben (2005), Comparison of coincident Multiangle Imaging Spectroradiometer and Moderate Resolution Imaging Spectroradiometer aerosol optical depths over land and ocean scenes containing Aerosol Robotic Network sites, *J. Geophys. Res.*, *110*, D10S07, doi:10.1029/2004JD004693.

Alexandrov, M., A. Lacis, B. Carlson, and B. Cairns (2002a), Derivation of 2D fields of aerosol and trace gases parameters by integrated analysis of multi-instrument MFRSR dataset from DOE ARM program CART site, in *Proc. SPIE*, *4539*, 277–288.

Bishop, C. H., and D. Hodyss (2009), Ensemble covariances adaptively localized with ECO-RAP. Part 1: Tests on simple error models, *Tellus A*, *61*, 84–96, doi:10.1111/j.1600-0870.2008.00371.x.

Björnsson, H., and S. A. Venegas (1997), *A Manual for EOF and SVD Analysis of Climate Data*, CCGCR Rep. 97–1, pp. 52, McGill University, Montréal, QC, Canada.

Bretherton, C. S., C. Smith, and J. M. Wallace (1992), An intercomparison of methods for finding coupled patterns in climate data, *J. Clim.*, *5*, 541–560.

Buehner, M., and M. Charron (2007), Spectral and spatial localization of background-error correlations for data assimilation, *Q. J. R. Meteorol. Soc.*, *133*, 615–630, doi:10.1002/qj.50.

Cermak, J., and R. Knutti (2009), Beijing Olympics as an aerosol field experiment, *Geophys. Res. Lett.*, *36*, L10806, doi:10.1029/2009GL038572.

Chin, M., et al. (2002), Tropospheric aerosol optical thickness from the GOCART model and comparisons with satellite and Sun photometer measurements, *J. Atom. Sci.*, *59*, 461–483.

Chu, D. A., Y. J. Kaufman, C. Ichoku, L. A. Remer, D. Tanré, and B. N. Holben (2002), Validation of MODIS aerosol optical depth retrieval over land, *Geophys. Res. Lett.*, *29*(12), 1617, doi:10.1029/2001GL013205.

Dey, S., S. N. Tripathi, R. P. Singh and B. N. Holben (2004), Influence of dust stroms on aerosol optical properties over the Indo-Gangetic basin, *J. Geophys. Res.*, *109*, D20211, doi:10.1029/2004JD004924.

Diner, D. J., et al. (1998), Multiangle Imaging SpectroRadiometer (MISR) escription and experiment overview, *IEEE Trans. Geosci. Remote. Sens.*, *36*, 1072–1087.

Duncan, B. N., R. V. Martin, A. C. Staudt, R. Yevich, and J. A. Logan (2003), Interannual and seasonal variability of biomass burning emissions constrained by satellite observations, *J. Geophys. Res.*, *108*(D2), 4040, doi:10.1029/2002JD002378.

Eck, T. F., B. N. Holben, J. S. Reid, O. Dubovik, A. Smirnov, N. T. O'Neill, I. Slutsker, and S. Kinne (1999), Wavelength dependence of the optical depth of biomass burning, urban, and desert dust aerosols, *J. Geophys. Res.*, *104*(D24), 31,333–31,349, doi:10.1029/1999JD900923.

Eck, T. F., et al. (2010), Climatological aspects of the optical properties of fine/coarse mode aerosol mixtures, *J. Geophys. Res.*, *115*, D19205, doi:10.1029/2010JD014002.

Eck, T. F., et al. (2013), A seasonal trend of single scattering albedo in southern African biomass-burning particles: Implications for satellite products and estimates of emissions for the world's largest biomass-burning source, *J. Geophys. Res. Atmos.*, *118*, 6414–6432, doi:10.1002/jgrd.50500.

Evan, A. T., D. J. Vimont, A. K. Heidinger, J. P. Kossin, and R. Bennartz (2009), The role of aerosols in the evolution of tropical North Atlantic Ocean temperature anomalies, *Science*, *324*, 778–781.

Evensen, G. (2003), The ensemble Kalman filter: Theoretical formulation and practical implementation, *Ocean Dyn.*, *53*(4), 343–367.

Foltz, G. R., and M. J. McPhaden (2008), Impact of Saharan dust on tropical north Atlantic SST, *J. Clim.*, *21*(19), 5048–5060.

Gao, Y., X. Liu, C. Zhao, and M. Zhang (2011), Emission controls versus meteorological conditions in determining aerosol concentrations in Beijing during the 2008 Olympic Games, *Atmos. Chem. Phys.*, *11*(23), 12,437–12,451.

García, O. E., J. P. Díaz, F. J. Expósito, A. M. Díaz, O. Dubovik, Y. Derimian, P. Dubuisson, and J.-C. Roger (2012), Shortwave radiative forcing and efficiency of key aerosol types using AERONET data, *Atmos. Chem. Phys.*, *12*, 5129–5145, doi:10.5194/acp-12-5129-2012.

Ginoux, P., D. Garbuzov, and N. C. Hsu (2010), Identification of anthropogenic and natural dust sources using Moderate Resolution Imaging Spectroradiometer (MODIS) Deep Blue level 2 data, *J. Geophys. Res.*, *115*, D05204, doi:10.1029/2009JD012398.

Guo, S., M. Hu, Q. Guo, X. Zhang, J. J. Schauer, and R. Zhang (2013), Quantitative evaluation of emission controls on primary and secondary organic aerosol sources during Beijing 2008 Olympics, *Atmos. Chem. Phys.*, *13*, 8303–8314, doi:10.5194/acp-13-8303-2013.

Hoelzemann, J. J., K. M. Longo, R. M. Fonseca, N. M. E. do Rosário, H. Elbern, S. R. Freitas, and C. Pires (2009), Regional representativity of AERONET observation sites during the biomass burning season in South America determined by correlation studies with MODIS Aerosol Optical Depth, *J. Geophys. Res.*, *114*, D13301, doi:10.1029/2008JD010369.

Holben, B. N., et al. (1998), AERONET—A federated instrument network and data archive for aerosol characterization, *Remote Sens. Environ.*, *66*, 1–16.

Hooghiemstra, P. B., M. C. Krol, T. T. van Leeuwen, G. R. van derWerf, P. C. Novelli, M. N. Deeter, I. Aben, and T. Röckmann (2012), Interannual variability of carbon monoxide emission estimates over South America from 2006 to 2010, *J. Geophys. Res.*, *117*, D15308, doi:10.1029/2012JD017758.

Hsu, N. C., S. C. Tsay, M. D. King, and J. R. Herman (2004), Aerosol properties over bright reflecting source regions, *IEEE Trans. Geosci. Remote Sens.*, *42*, 557–569.

Hsu, N. C., S. C. Tsay, M. D. King, and J. R. Herman (2006), Deep blue retrievals of Asian aerosol properties during ACE-Asia, *IEEE Trans. Geosci. Remote Sens.*, *44*, 3180–3195.

Hubanks, P., M., King, S. Platnick, and R. Pincus (2008), MODIS atmosphere L3 gridded product algorithm theoretical basis document Collection 005 Version 1.1, Tech. Rep. ATBD-MOD-30, NASA.

Hyer, E. J., J. S. Reid, and J. Zhang (2011), An over-land aerosol optical depth data set for data assimilation by filtering, correction, and aggregation of MODIS Collection 5 optical depth retrievals, *Atmos. Meas. Tech.*, *4*, 379–408, doi:10.5194/amt-4-379-2011.

Ichoku, C., D. A. Chu, S. Mattoo, Y. J. Kaufman, L. A. Remer, D. Tanré, I. Slutsker, and B. N. Holben (2002), A spatio-temporal approach for global validation and analysis of MODIS aerosol products, *Geophys. Res. Lett.*, *29*(12), 1616, doi:10.1029/2001GL013206.

Jethva, H., S. K. Satheesh, and J. Srinivasan (2007), Assessment of second-generation MODIS aerosol retrieval (Collection 005) at Kanpur, India, *Geophys. Res. Lett.*, *34*, L19802, doi:10.1029/2007GL029647.

Jung, E., B. Albrecht, J. M. Prospero, H. H. Jonsson, and S. M. Kreidenweis (2013), Vertical structure of aerosols, temperature, and moisture associated with an intense African dust event observed over the eastern Caribbean, *J. Geophys. Res. Atmos.*, *118*, 4623–4643, doi:10.1002/jgrd.50352.

Kahn, R. A., B. J. Gaitley, J. V. Martonchik, D. J. Diner, K. A. Crean, and B. Holben (2005), Multiangle Imaging Spectroradiometer (MISR) global aerosol optical depth validation based on 2 years of coincident Aerosol Robotic Network (AERONET) observations, *J. Geophys. Res.*, *110*, D10S04, doi:10.1029/2004JD004706.

Kahn, R. A., D. L. Nelson, M. J. Garay, R. C. Levy, M. A. Bull, D. J. Diner, J. V. Martonchik, S. R. Paradise, E. G. Hansen, and L. A. Remer (2009), MISR aerosol product attributes and statistical comparisons with MODIS, *Geosci. Remote Sens., IEEE Trans. on*, *47*, 4095–4114.

Kahn, R. A., B. J. Gaitley, M. J. Garay, D. J. Diner, T. F. Eck, A. Smirnov, and B. N. Holben (2010), Multiangle Imaging SpectroRadiometer global aerosol product assessment by comparison with the Aerosol Robotic Network, *J. Geophys. Res.*, *115*, D23209, doi:10.1029/2010JD014601.

Kaskaoutis, D. G., S. K. Kharol, P. R. Sinha, R. P. Singh, K. V. S. Badarinath, W. Mehdi, and M. Sharma (2011), Contrasting aerosol trends over South Asia during the last decade based on MODIS observations, *Atmos. Meas. Tech. Discuss*, *4*, 5275–5323.

Kaufman, Y. J., D. Tanré, and O. Boucher (2002), A satellite view of aerosols in the climate system, *Nature*, *419*(6903), 215–223.

Kiehl, J. T., and V. Ramanathan (2006), *Frontiers of Climate Modeling*, Cambridge Univ. Press, New York, USA.

Kinne, S., et al. (2006), An AeroCom initial assessment–optical properties in aerosol component modules of global models, *Atmos. Chem. Phys.*, *6*, 1815–1834.

Kishcha, P., B. Starobinets, and P. Alpert (2007), Latitudinal variations of cloud and aerosol optical thickness trends based on MODIS satellite data, *Geophys. Res. Lett.*, *34*, L05810, doi:10.1029/2006GL028796.

Kokhanovsky, A. A., F. M. Breon, A. Cacciari, E. Carboni, D. Diner, W. Di Nicolantonio, and W. von Hoyningen-Huene (2007), Aerosol remote sensing over land: A comparison of satellite retrievals using different algorithms and instruments, *Atmos. Res.*, *85*(3), 372–394.

Levy, R. C., L. A. Remer, S. Mattoo, E. F. Vermote, and Y. J. Kaufman (2007), Second-generation operational algorithm: Retrieval of aerosol properties over land from inversion of Moderate Resolution Imaging Spectroradiometer spectral reflectance, *J. Geophys. Res.*, *112*, D13211, doi:10.1029/2006JD007811.

Levy, R. C., G. G. Leptoukh, R. Kahn, V. Zubko, A. Gopalan, and L. A. Remer (2009), A critical look at deriving monthly aerosol optical depth from satellite data, *Geosci. Remote Sens., IEEE Trans. on*, *47*(8), 2942–2956.

Levy, R. C., L. A. Remer, R. G. Kleidman, S. Mattoo, C. Ichoku, R. Kahn, and T. F. Eck (2010), Global evaluation of the Collection 5 MODIS dark-target aerosol products over land, *Atmos. Chem. Phys.*, *10*, 10,399–10,420, doi:10.5194/acp-10-10399-2010.

Levy, R. C., S. Mattoo, L. A. Munchak, L. A. Remer, A. M. Sayer, F. Patadia, and N. C. Hsu (2013), The Collection 6 MODIS aerosol products over land and ocean, *Atmos. Meas. Tech.*, *6*, 2989–3034, doi:10.5194/amt-6-2989-2013.

Li, J., L. Liu, A. A. Lacis, and B. E. Carlson (2010), An optimal fitting approach to improve the GISS ModelE aerosol optical property parameterization using AERONET data, *J. Geophys. Res.*, *115*, D16211, doi:10.1029/2010JD013909.

Li, J., B. E. Carlson, and A. A. Lacis (2011), El Niño-Southern Oscillation correlated aerosol Ångström Exponent anomaly over the tropical Pacific discovered in satellite measurements, *J. Geophys. Res.*, *116*, D20204, doi:10.1029/2011JD015733.

Li, J., B. E. Carlson, and A. A. Lacis (2013), Application of spectral analysis techniques in the inter-comparison of aerosol data. Part I: An EOF approach to analyze the spatial-temporal variability of aerosol optical depth using multiple remote sensing data sets, *J. Geophys. Res. Atmos.*, *118*, 8640–8648, doi:10.1002/jgrd.50686.

Liu, L., A. A. Lacis, B. E. Carlson, M. I. Mishchenko, and B. Cairns (2006), Assessing Goddard Institute for Space Studies ModelE aerosol climatology using satellite and ground-based measurements: A comparison study, *J. Geophys. Res.*, *111*, D20212, doi:10.1029/2006JD007334.

Lu, Z., D. G. Streets, Q. Zhang, S. Wang, G. R. Carmichael, Y. F. Cheng, C. Wei, M. Chin, T. Diehl, and Q. Tan (2010), Sulfur dioxide emissions in China and sulfur trends in East Asia since 2000, *Atmos. Chem. Phys.*, *10*, 6311–6331.

Mace, G. G., et al. (2006), Cloud radiative forcing at the Atmospheric Radiation Measurement Program Climate Research Facility: 1. Technique, validation, and comparison to satellite-derived diagnostic quantities, *J. Geophys. Res.*, *111*, D11S90, doi:10.1029/2005JD005921.

Martins, J. V., D. Tanré, L. Remer, Y. Kaufman, S. Mattoo, and R. Levy (2002), MODIS Cloud screening for remote sensing of aerosols over oceans using spatial variability, *Geophys. Res. Lett.*, *29*(12), 1619, doi:10.1029/2001GL013252.

Martonchik, J. V., D. J. Diner, R. Kahn, B. Gaitley, and B. N. Holben (2004), Comparison of MISR and AERONET aerosol optical depths over desert sites, *Geophys. Res. Lett.*, *31*, L16102, doi:10.1029/2004GL019807.

Martonchik, J. V., R. A. Kahn, and D. J. Diner (2009), Retrieval of aerosol properties over land using MISR observations, in *Satellite Aerosol Remote Sensing Over Land*, pp. 267–293, Springer, Berlin Heidelberg.

Mishchenko, M. I., I. V. Geogdzhayev, W. B. Rossow, B. Cairns, B. E. Carlson, A. A. Lacis, L. Liu, and L. D. Travis (2007), Long-term satellite record reveals likely recent aerosol trend, *Science*, *315*, 1543–1543.

Petrenko, M., R. Kahn, M. Chin, A. Soja, and T. Kucsera (2012), The use of satellite-measured aerosol optical depth to constrain biomass burning emissions source strength in the global model GOCART, *J. Geophys. Res.*, *117*, D18212, dio:10.1029/2012JD17870.

Prasad, A. K., and R. P. Singh (2007), Comparison of MISR-MODIS aerosol optical depth over the Indo-Gangetic basin during the winter and summer seasons (2000–2005), *Remote Sens. Environ.*, *107*, 109–119.

Remer, L. A., Y. J. Kaufman, D. Tanré, S. Mattoo, D. A. Chu, J. Martins, and B. N. Holben (2005), The MODIS aerosol algorithm, products, and validation, *J. Geophys. Res.*, *62*, D10S18, doi:10.1029/2004JD004611.

Remer, L. A., et al. (2008), Global aerosol climatology from the MODIS satellite sensors, *J. Geophys. Res.*, *113*, D14S07, doi:10.1029/2007JD009661.

Shi, Y., J. Zhang, J. S. Reid, E. J. Hyer, T. F. Eck, B. N. Holben, and R. A. Kahn (2011), A critical examination of spatial biases between MODIS and MISR aerosol products – Application for potential AERONET deployment, *Atmos. Meas. Tech.*, *4*, 2823–2836, doi:10.5194/amt-4-2823-2011.

Singh, R. P., S. Dey, S. N. Tripathi, V. Tare, and B. N. Holben (2004), Variability of aerosol parameters over Kanpur city, northern India, *J. Geophys. Res.*, *109*, D23206, doi:10.1029/2004JD004966.

Smirnov, A., B. N. Holben, T. F. Eck, O. Dubovik, and I. Slutsker (2000), Cloud-screening and quality control algorithms for the AERONET database, *Remote Sens. Environ.*, *73*, 337–349.

Torres, O., Z. Chen, H. Jethva, C. Ahn, S. R. Freitas, and P. K. Bhartia (2010), OMI and MODIS observations of the anomalous 2008–2009 Southern Hemisphere biomass burning seasons, *Atmos. Chem. Phys.*, *10*, 3505–3513.

Tosca, M. G., J. T. Randerson, C. S. Zender, M. G. Flanner, and P. J. Rasch (2010), Do biomass burning aerosols intensify drought in equatorial Asia during El Nino?, *Atmos. Chem. Phys.*, *10*, 3515–3528.

Tripathi, S. N., S. Dey, A. Chandel, S. Srivastava, R. P. Singh, and B. N. Holben (2005), Comparison of MODIS and AERONET derived aerosol optical depth over the Ganga Basin, India, *Ann. Geophys.*, *23*, 1093–1101, doi:10.5194/angeo-23-1093-2005.

Wang, K., R. E. Dickinson, and S. Liang (2009), Clear sky visibility has decreased over land globally from 1973 to 2007, *Science*, *323*, 1468–1470.

Wang, T., W. Nie, J. Gao, L. K. Xue, X. M. Gao, X. Wang, and W. X. Wang (2010), Air quality during the 2008 Beijing Olympics: Secondary pollutants and regional impact, *Atmos. Chem. Phys.*, *10*(16), 7603–7615.

Xin, J., et al. (2007), Aerosol optical depth (AOD) and Ångström exponent of aerosols observed by the Chinese Sun Hazemeter Network from August 2004 to September 2005, *J. Geophys. Res.*, *112*, D05203, doi:10.1029/2006JD007075.

Yoon, J., W. von Hoyningen-Huene, A. A. Kokhanovsky, M. Vountas, and J. P. Burrows (2012), Trend analysis of aerosol optical thickness and Ångström exponent derived from the global AERONET spectral observations, *Atmos. Meas. Tech.*, *5*, 1271–1299.

Yu, X., B. Zhu, and M. Zhang (2009), Seasonal variability of aerosol optical properties over Beijing, *Atmos. Environ.*, *43*, 4095–4101.

Zhang, J., and J. S. Reid (2006), MODIS aerosol product analysis for data assimilation: Assessment of over-ocean level 2 aerosol optical thickness retrievals, *J. Geophys. Res.*, *111*, D22207, doi:10.1029/2005JD006898.